PAPER • OPEN ACCESS

Energy landscapes for a modified repulsive Weeks–Chandler–Andersen potential

View the article online for updates and enhancements.

Energy landscapes for a modified repulsive Weeks–Chandler–Andersen potential

Atreyee Banerjee[1,2] and **David J Wales**[1]

[1] Yusuf Hamied Department of Chemistry, University of Cambridge, Lensfield Road, Cambridge CB2 1EW, United Kingdom
[2] Max Planck Institute for Polymer Research, Ackermannweg 10, 55128 Mainz, Germany

E-mail: banerjeea@mpip-mainz.mpg.de and dw34@cam.ac.uk

CrossMark

Abstract

The short-range nature of the repulsive Weeks–Chandler–Anderson (WCA) potential can create free particles/rattlers in a condensed system. The presence of rattlers complicates the analysis of the energy landscape due to extra zero-frequency normal modes. By employing a long-range Gaussian tail modification, we remove the rattlers without changing the structure and the dynamics of the system, and successfully describe the potential energy landscape in terms of minima and transition states. This coarse-grained description of the landscape and the dynamical properties of the modified potential exhibit characteristic signatures of glass-forming liquids. However, we show that despite having qualitatively similar behaviour, the modified WCA potential is less frustrated compared to its attractive counterpart.

Keywords: energy landscape, supercooled liquid, glass, structure dynamics, dis-connectivity graph

(Some figures may appear in colour only in the online journal)

1. Introduction

If crystallisation is avoided, liquids enter into a supercooled state upon fast cooling. The atomic structure of the metastable supercooled state remains almost unaffected while cooling, however, the dynamics differ quite significantly. There are different approaches to understand the origin of the sharp rise of viscosity and relaxation time on cooling [1]: one is based an on kinetic arrest [2], while complementary approaches consider the underlying potential energy landscape (PEL) [3–6].

The dynamical properties (X) usually follow Arrhenius behaviour with $X \propto \exp(\pm E/T)$ for a constant activation energy, E at high temperature. On cooling, the relationship deviates from Arrhenius behaviour and the enhanced growth of dynamical properties commonly fits reasonably well to a Vogel–Fulcher–Tammann (VFT) equation [7–9], where $X \propto \exp(\pm E/(T - T_{\mathrm{VFT}}))$, with T_{VFT} the singularity temperature. The dynamical growth can also be fitted to other forms without singularities [10, 11]. For some liquids, commonly referred to as 'strong', the Arrhenius behaviour holds down to low temperature. In contrast, liquids with super-Arrhenius growth are classified as 'fragile' [12, 13]. The strong liquids include network glass formers, such as silica and germanium oxides, while the fragile liquids include binary Lennard–Jones (BLJ) mixtures and a variety of molecular glasses, such as orthoterphenyl [14–18].

In the context of glasses, the PEL was probably first considered by Goldstein [19] in terms of multiple local minima connected by transition states. As shown in previous studies, the dynamical arrest at lower temperatures is attributed to neighbourhood cage formation. Rabani *et al* measured the cage-rattling timescale, and the cage-breaking timescale has been directly connected to super-Arrhenius behaviour [20]. While caged, the system is trapped in local minima with a lower escape probability to cross a relatively high barrier cor-

responding to cage-breaking, producing a longer timescale for relaxation. Heuer *et al* defined metabasins as a super-structure in the PEL, which are related to the slow dynamics [6, 21]. de Souza *et al* numerically connected the productive cage breaking rearrangements to transport properties [22].

In liquid state theory, the structure-dynamics relationship is well-established [23] and the repulsive part of the poten-tial is often connected to the structure of the liquid [24]. The Weeks–Chandler–Andersen (WCA) potential was derived to compare the repulsive part of the Lennard–Jones (LJ) potential to a hard-sphere system, while the attractive part was con-sidered as a perturbation [25]. The WCA potential is known to reproduce the structural properties of the LJ potential to some extent while the dynamical properties vary quite signifi-cantly [26–28]. Some of microscopic theories fail to predict the structure-dynamics relationship [29, 30], while a recent theory predicts the correct dynamical temperature [31]. Empir-ical relationships such as the Rosenfeld relation [32] hold at the high temperature limit, while the Adam–Gibbs relation [33] describes the behaviour quite well in the low temperature limit for the WCA system [18, 28]. More recently, a careful finite size analysis predicted long-range structure formation in LJ system compared to its repulsive counterpart [34]. How-ever, a clear basis for the structure-dynamics relationship is still missing. As the WCA potential consists of only the repul-sive part, it imitates the hard-sphere system and is widely used in molecular dynamics (MD) studies due to the continuity of the potential. In many systems, including colloids [35, 36], the WCA potential is often used to investigate distinct crystalline structures.

In this work, we aim to characterize the PEL for the repul-sive WCA system of a dense liquid. Due to the short-range nature of the WCA potential, the system can include rattlers, which contribute extra zero-frequency modes in the density of states, and complicate a description in terms of the sta-tionary points. To address this issue we modify the potential with the addition of a Gaussian tail, and show that we can avoid the numerical problems, while the structure and dynam-ics remain almost unaltered by the tail correction. We find that the time-dependent diffusivity follows similar behaviour to other glass-forming liquids. Finally, we visualise the PEL, which exhibits multiple competing minima, and compare it with the LJ counterpart.

The paper is organized as follows: the computational details are given in section 2 where we describe the tail correction. In section 3 we present our results. Section 4 contains the conclusions.

2. Computational details

2.1. The potential modification

We performed MD simulations of a 256 particle binary mixture of 204 A and 52 B atoms, interacting according to the repulsive counterpart WCA of the LJ potential in a periodically repeated cell [25, 37]. The interatomic pair potential between species α

and β, with $\alpha, \beta = $ A, B, $U_{\alpha\beta}^{\mathrm{WCA}}(r; \sigma_{\alpha\beta}, \epsilon_{\alpha\beta})$ is described by a shifted and truncated LJ potential:

$$
\begin{aligned}
& U_{\alpha\beta}^{\mathrm{WCA}}(r; \sigma_{\alpha\beta}, \epsilon_{\alpha\beta}) \\
& = \begin{cases} U_{\alpha\beta}^{\mathrm{LJ}}(r; \sigma_{\alpha\beta}, \epsilon_{\alpha\beta}) - U_{\alpha\beta}^{\mathrm{LJ}}(r_{\alpha\beta}^{\mathrm{c}}; \sigma_{\alpha\beta}, \epsilon_{\alpha\beta}), & r \leqslant r_{\alpha\beta}^{\mathrm{c}}, \\ 0, & r > r_{\alpha\beta}^{\mathrm{c}}, \end{cases}
\end{aligned}
$$
$$(1)$$

where $U_{\alpha\beta}^{\mathrm{LJ}}(r; \sigma_{\alpha\beta}, \epsilon_{\alpha\beta}) = 4\epsilon_{\alpha\beta}[(\sigma_{\alpha\beta}/r)^{12} - (\sigma_{\alpha\beta}/r)^6]$ and $r_{\alpha\beta}^{\mathrm{c}}$ is equal to the position of the minimum in $U_{\alpha\beta}^{\mathrm{LJ}}$ for the WCA counterpart. Length, temperature and time are given in units of σ_{AA}, $\epsilon_{\mathrm{AA}}/k_{\mathrm{B}}$ and $\sqrt{(m_{\mathrm{A}}\sigma_{\mathrm{AA}}^2/\epsilon_{\mathrm{AA}})}$, respectively. Here we have simulated the Kob–Andersen model [37] with interac-tion parameters $\sigma_{\mathrm{AA}} = 1.0$, $\sigma_{\mathrm{AB}} = 0.8$, $\sigma_{\mathrm{BB}} = 0.88$, $\epsilon_{\mathrm{AA}} = 1$, $\epsilon_{\mathrm{AB}} = 1.5$, $\epsilon_{\mathrm{BB}} = 0.5$, $m_{\mathrm{A}} = m_{\mathrm{B}} = 1.0$. We performed MD sim-ulations in the canonical ensemble (NVT) at densities $\rho = 1.4$ for the WCA potential.

Due to the shorter-range cutoff of the original WCA poten-tial, we observed that some of the configurations were not converged properly during minimisation. This convergence problem has been reported earlier for polydisperse WCA sys-tems [38]. The existence of rattlers creates ambiguity in the coarse-grained description of the landscape based on minima and transition states. In order to tackle this numerical problem, we modified the WCA potential by adding a Gaussian tail modification up to a longer cutoff r_2 (figure 1). We make sure the potential and its derivative are zero at the longer cutoff. The modified WCA (mWCA) potential with tail correction U_{corr} is written as,
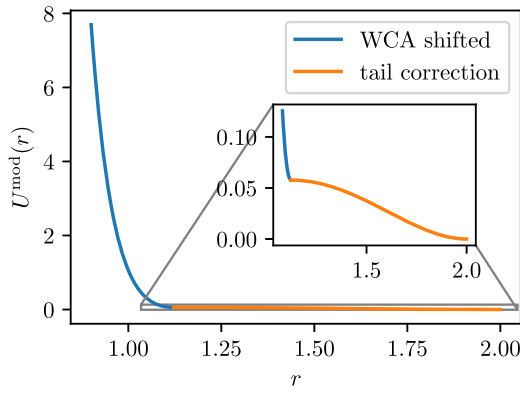
$$
\begin{aligned}
& U_{\alpha\beta}^{\mathrm{mod}}(r) \\
& = \begin{cases} U_{\alpha\beta}^{\mathrm{WCA}}(r; \sigma_{\alpha\beta}, \epsilon_{\alpha\beta}) + U_{\alpha\beta}^{\mathrm{corr}}(r_{\alpha\beta}^{\mathrm{c}}; \sigma_{\alpha\beta}, \epsilon_{\alpha\beta}), & r < r_{\alpha\beta}^{\mathrm{c}}, \\ U_{\alpha\beta}^{\mathrm{corr}}(r; \sigma_{\alpha\beta}, \epsilon_{\alpha\beta}), & r_{\alpha\beta}^{\mathrm{c}} \leqslant r \leqslant r_2, \end{cases}
\end{aligned}
$$
$$(2)$$

where the tail corrected potential term is,

$$
\begin{aligned}
U_{\alpha\beta}^{\mathrm{corr}}(r; \sigma_{\alpha\beta}, \epsilon_{\alpha\beta}) = & \Delta\epsilon_{\alpha\beta} \exp\left(-\frac{(r - r_{\alpha\beta}^{\mathrm{c}})^2}{2\sigma_{\alpha\beta}^2}\right) \\
& + A_0 + A_1(r - r_{\alpha\beta}^{\mathrm{c}})^2
\end{aligned}
$$
$$(3)$$

with A_0, A_1 constants. We evaluate the constants by setting the potential and its first derivative to zero at the long cutoff, so that $U_{\alpha\beta}^{\mathrm{corr}}(r_2; \sigma_{\alpha\beta}, \epsilon_{\alpha\beta}) = 0$ and $\partial U_{\alpha\beta}^{\mathrm{corr}}(r_2; \sigma_{\alpha\beta}, \epsilon_{\alpha\beta})/\partial r = 0$. The partial derivative is given by

$$
\begin{aligned}
\frac{\partial U_{\alpha\beta}^{\mathrm{corr}}(r; \sigma_{\alpha\beta}, \epsilon_{\alpha\beta})}{\partial r} = & \Delta\epsilon_{\alpha\beta} \exp\left(-\frac{(r - r_{\alpha\beta}^{\mathrm{c}})^2}{2\sigma_{\alpha\beta}^2}\right) \\
& \times \frac{-2(r - r_{\alpha\beta}^{\mathrm{c}})}{2\sigma_{\alpha\beta}^2} + 2A_1(r - r_{\alpha\beta}^{\mathrm{c}}).
\end{aligned}
$$

Figure 1. The modified WCA (mWCA) potential, $U^{\mathrm{mod}}(r)$, as given by equation (2). In the inset we magnify the tail corrected part of the potential. The yellow line corresponds to the Gaussian tail correction as given in equation (3).

On simplification at $r = r_2$ we obtain

$$A_1 = \frac{\Delta\epsilon_{\alpha\beta}}{2\sigma_{\alpha\beta}^2} \exp\left(-\frac{(r_2 - r_{\alpha\beta}^c)^2}{2\sigma_{\alpha\beta}^2}\right).$$

Using this A_1 value we obtain

$$A_0 = -\Delta\epsilon_{\alpha\beta} \exp\left(-\frac{(r_2 - r_{\alpha\beta}^c)^2}{2\sigma_{\alpha\beta}^2}\right)$$
$$- \frac{\Delta\epsilon_{\alpha\beta}(r_2 - r_{\alpha\beta}^c)^2}{2\sigma_{\alpha\beta}^2} \exp\left(-\frac{(r - r_{\alpha\beta}^c)^2}{2\sigma_{\alpha\beta}^2}\right)$$

$$A_0 = -\Delta\epsilon_{\alpha\beta} \exp\left(-\frac{(r_2 - r_{\alpha\beta}^c)^2}{2\sigma_{\alpha\beta}^2}\right)\left[1 + \frac{(r_2 - r_{\alpha\beta}^c)^2}{2\sigma_{\alpha\beta}^2}\right].$$

We denote the mWCA potential $U_{\alpha\beta}^{\mathrm{mod}}(r)$ as mWCA and simulated the system with this potential for further analysis. We have chosen $r_2 = 2\sigma_{\mathrm{AA}}$, and $\Delta\epsilon_{\alpha\beta} = \epsilon_{\alpha\beta}$ to remove the zero frequency modes.

2.2. Potential energy landscapes

The PEL was explored using geometry optimization to characterize local minima and the pathways that connect them. We quenched the MD trajectory at each step using the L-BFGS method [39] until the root-mean-square gradient fell below 10^{-6} reduced units, and connected the successive quenched minima in the trajectory using the doubly-nudged [40, 41] elastic band [42–45] method for double-ended searches to locate transition state candidates, which were refined using hybrid eigenvector-following [40, 46, 47]. The connectivity was then established by calculating approximate steepest-descent paths for each transition state. Additional candidates for connection attempts were then chosen using the missing connection algorithm [48], until the endpoints were successfully linked. This approach is implemented in the OPTIM program [49], which finds the pathways between two successive quenched minima. The pathways can consist of a single transition state or a series of transition states and intervening minima. Hence it is essential to refine transition state candidates

and establish the connectivity following the initial DNEB calculation [50]. Once we have the database of minima and transition states, we visualise the connectivity of the landscape using disconnectivity graph analysis [51, 52]. The complex topology of the higher dimensional landscape can be visualised using these tree graphs, where the vertical axis corresponds to increasing energy. Disconnectivity graphs can display all the minima, and faithfully represent the lowest barriers separating them. This approach is implemented in the open source disconnectionDPS program [53].

3. Result

3.1. Structure and dynamics of the modified potential

We analyse the structure and dynamics of the tail modified potential by calculating the radial distribution function and diffusion coefficient. In figures 2(a) and (b) we plot the radial distribution function of the original WCA potential at a high and a low temperature, and compare them with the corresponding tail-mWCA potential. We observe that the radial distribution function remains similar at high temperature. However, the BB part of the radial distribution function slightly differs at low temperatures. B particles, which are smaller in size, behave as rattlers at low densities, due to a shorter interaction range. The tail modification provides a weak but longer interaction contribution, thus it affects mostly the smaller size particles, which have relatively shorter interaction range cutoff in the original potential.

The diffusion coefficient, D, is calculated using the Einstein relationship in the ergodic limit as,

$$D = \lim_{t \to \infty} \frac{1}{6t} \langle \Delta\mathbf{r}_i(t)^2 \rangle, \tag{4}$$

where, $\langle \cdot \rangle$ denotes the ensemble average over atoms i. We observe that the dynamics with and without the tail correction remain very similar throughout the temperature range of interest. A slight deviation is observed in the low-temperature regime. The presence of a longer cutoff may increase the number of nearest-neighbours and, as a result, the peak height for the B-type particles increases slightly and their diffusivity is reduced compared to the original potential. However, overall, the results show that the tail modification is a weak perturbation, so that we effectively retain a system with similar thermodynamic and dynamical properties.

The vibrational density of states of the quenched configurations was calculated as

$$P(\omega) = \frac{1}{3N - 3} \sum_l \langle \delta(\omega - \omega_l) \rangle, \tag{5}$$

where ω_l is the angular frequency of mode l in reduced units. In figure 3 we show that although the zero frequency modes disappear with the tail modification, the overall density profile does not change significantly. The zero-frequency modes correspond to regions of the PEL where one or more particles have no interaction with the others, and so the energy is invariant
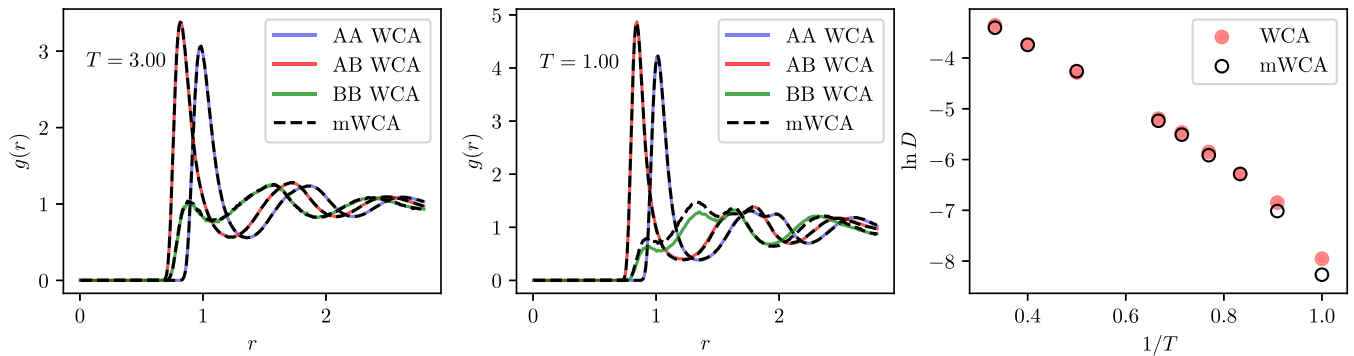
Figure 2. The partial radial distribution function for original WCA and tail modified (mWCA) at (a) high temperature ($T = 3.00$), and (b) low temperature ($T = 1.00$). (c) The diffusivity calculated using equation (4) for both systems. The results show that the structure and dynamics remain mostly unaltered by the tail modification. At low temperature, a small increase of the peak height in the radial distribution function of the B–B particles and a slight slow down of the diffusivity are observed.
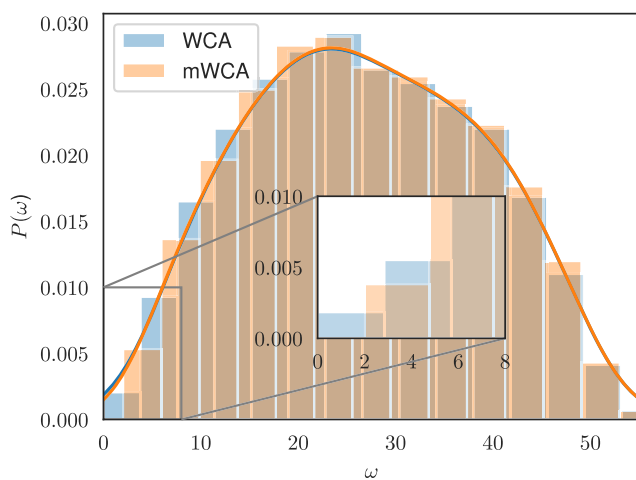
Figure 3. The density of states $P(\omega)$ in reduced units for original WCA and tail modified (mWCA) potentials. The zero frequency modes disappear with the tail correction. However, the overall density profiles are practically the same.

with respect to infinitesimal displacements in the corresponding degrees of freedom. Addition of a long-range Gaussian tail restores some small interactions for these particles, so that the zero-frequency modes are removed, which solves the numerical problems. We can now calculate the transition states effectively between the minimized configurations, as described in section 2. Note that one can perform instantaneous normal mode analysis without quenching the system, where a large fraction of modes often have imaginary frequencies [54]. In our case, we perform the normal mode analysis for the local minima, which have only positive vibrational frequencies by construction.

3.2. Diffusion analysis

In this section, we report some other dynamical properties commonly observed for glassy systems, such as the time-dependent diffusivity. The nonergodic diffusion constant, $D(\tau)$, is calculated over shorter, nonergodic time intervals, τ [10, 55], and we consider the average value over an ergodic

trajectory. The true diffusion coefficient D is recovered when the interval τ is large enough. If the total trajectory is divided into m shorter time intervals, τ, then we define the diffusion constant for time scale τ [10, 55] as

$$D(\tau) \equiv \lim_{t \to \infty} \frac{1}{6t} \langle \Delta \mathbf{r}_i(t, \tau)^2 \rangle, \qquad (6)$$

where the mean squared displacement $\Delta \mathbf{r}_i(t, \tau)^2 = \sum_{j=1}^{m} \Delta \mathbf{r}_i(j)^2$ with $m\tau = t$, and the displacement of particle i in time interval j is $\Delta \mathbf{r}_i(j) = \mathbf{r}_i(j\tau) - \mathbf{r}_i(j\tau - \tau)$.

We find that the diffusivity follows Arrhenius behaviour down to much lower temperature when we consider shorter time windows. At high temperatures, the shorter time windows are a reasonably good approximation to the true diffusivity. However, at low temperatures the deviation is considerable. The short time windows significantly overestimate the diffusivity due to the neglect of correlated motions [10, 55, 56]. As expected, local ergodicity only emerges over a longer timescale for the low-temperature range. However, as in previous work [10, 55, 56], a mean-field like diffusion coefficient $D^*_{\text{corr}}(\tau)$ can be obtained from combining a correction factor with the short time diffusion coefficient. The correction factor is given by

$$\langle \Delta \mathbf{r}_i^2(t, \tau) \rangle \approx \sum_{j=1}^{m} \langle \Delta \mathbf{r}_i(j)^2 \rangle (1 + 2\langle \cos \theta_{j,j+1} \rangle),$$

$$D^*_{\text{corr}}(\tau) = D(\tau)(1 + 2\langle \cos \theta_{j,j+1} \rangle).$$

$\theta_{j,j+1}$ is the angle between the displacement vectors for atom i in intervals j and $j + 1$. Here we assume the displacement for every atom in every interval has the same magnitude, thus $D^*_{\text{corr}}(\tau)$ provides a mean-field type description. Similar to other systems considered in previous work, the correction term becomes more negative on lowering the temperature. In figure 4(b), we plot $D^*_{\text{corr}}(\tau)$ and find that it gives a reasonable description of the true diffusion, even for small time intervals. This result is consistent with our earlier analysis of time-dependent diffusivity for the original WCA system [56] and for other glass forming liquids [10, 16, 17, 55].
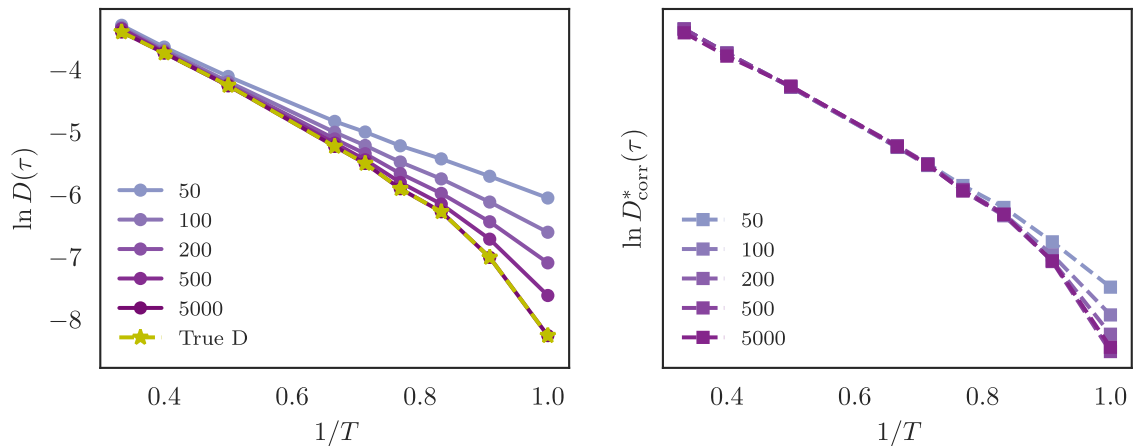
Figure 4. (a) The time dependent diffusion coefficients $D(\tau)$ and (b) the mean-field type approximation $D^*_{\text{corr}}(\tau)$ for the mWCA system with a range of time windows $\tau = 50, 100, 200, 500, 1000, 5000$ MD steps and time step $dt = 0.005$ in reduced units. We observe at $\tau = 5000$ that $D(\tau)$ has converged to the true diffusion constant calculated using equation (4). At high temperatures $D(\tau)$ is a reasonable estimate, but at lower temperature with shorter time windows it gives an overestimate.

3.3. Energy landscapes

We follow the protocol described in section 2 to visualize the PEL of the WCA system. We used the quenched trajectory from the MD simulation at a temperature $T = 0.95$. The coordinates were saved every ten MD steps with each time step 0.001 in reduced units. Since we follow the MD trajectory, the order in which the minima of the PEL are visited by the system during the time evolution is maintained. In figure 5, we plot the disconnectivity graph for the WCA system with the tail modification. The landscape is highly frustrated [22] with multiple minima and transition states and a wide range of energy values. We did not observe crystallisation, or any low energy crystalline minima, in these calculations.

WCA systems at low densities are prone to crystallise [34, 58]. It would be interesting in future work to study lower densities with the modified potential in order to include the crystalline state in the disconnectivity graph.

The degree of 'frustration' in the PEL can be quantified by a metric that describes the existence of competing low-lying minima and their separation in terms of energy barriers [57]. Usually, glass formers exhibit higher frustration and structure-seeker systems, such as magic number clusters, have lower frustration. More recently, the fragile BLJ systems were compared with a strong liquid SiO_2. Despite exhibiting similar disconnectivity graphs, the frustration metric had a lower value for the latter system [17]. The landscape entropy [59–61], calculated from the potential energy density of minima, has also been used to compare systems with different degrees of fragility [28]. The rate at which the landscape entropy decreases with temperature, sometimes termed 'thermodynamic fragility', is higher for LJ systems compared to the WCA counterpart [28, 62]. The frustration metric used in the present study is a complementary measure designed to quantify the mutual accessibility by explicit consideration of the barriers between local minima [57].
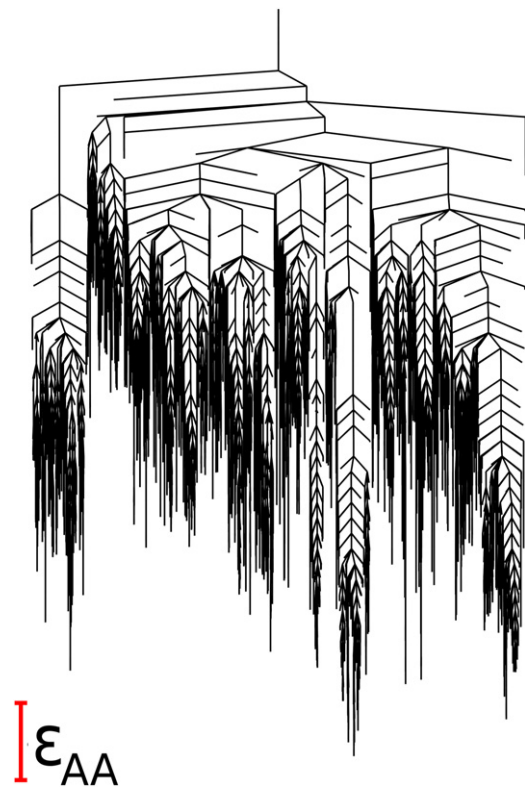
Figure 5. Disconnectivity graph for the mWCA system with the tail correction at $\rho = 1.4$.

To classify the systems, de Souza *et al* described a renormalised frustration index $\widetilde{f}(T)$ [57] after removing the temperature dependence of the lowest minimum. They observed that $\widetilde{f}(T) < 1$ for the structure-seekers, whereas the frustrated landscapes, including BLJ, have $1 > \widetilde{f}(T) > 50$. It is apparent that the mWCA system has a multifunnel structure, as expected for a glassy system. In figure 6 we show that the barrier crossing ability decreases upon lowering the temperature. However, when compared with BLJ systems, we observe
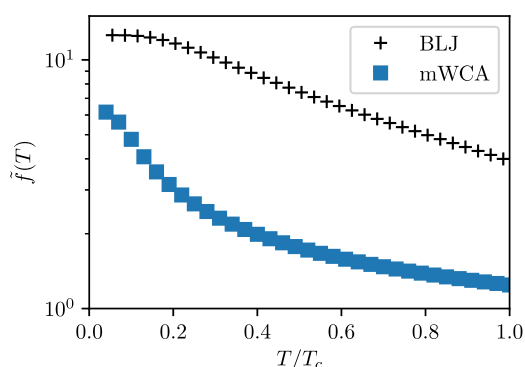
Figure 6. The renormalised frustration index for BLJ [57] and mWCA system.

that the values are lower throughout the temperature range, and the system is less frustrated, indicating a more uniform organised landscape of smaller metabasins.

4. Conclusion

The WCA potential was first introduced by shifting the attractive LJ potential at the cutoff of the energy minimum [25]. The short range and continuous nature of this repulsive potential make it popular for computer simulation studies, including colloids [36], polymers with excluded volume interactions [63], and glassy systems [28, 56]. We found, however, that the short range nature of the potential leads to rattlers in the system, which contribute extra zero frequency modes to the density of states, complicating analysis of the energy landscape. To circumvent this problem, we add a Gaussian tail to the original WCA potential that is long enough to remove the free particles, but at the same time weak enough to retain the structure and dynamics of the original WCA system. As a consequence, we observed that the extra zero frequency modes are successfully removed, while the overall behaviour of interest is conserved. The system with a mWCA potential exhibits characteristic behaviour of glass forming liquids, such as super-Arrhenius diffusivity reduction, frustrated energy landscapes, higher frustration index, etc. It exhibits somewhat lower frustration compared to its attractive counterpart. As for BLJ systems, we find that diffusion constants calculated over short time intervals exhibit Arrhenius behaviour, but the true super-Arrhenius temperature dependence can be recovered using a correction term that describes the correlation between displacements in neighbouring time windows. This correlation factor is negative, and the magnitude increases with decreasing temperature, producing super-Arrhenius behaviour.

Identification of crystalline states for the mWCA potential at lower densities, and exploring the energy landscape, are interesting areas to be investigated in the future.

Acknowledgments

ORCID iDs

Atreyee Banerjee ![ORCID] https://orcid.org/0000-0002-0518-609X
David J Wales ![ORCID] https://orcid.org/0000-0002-3555-6645

References

[1] Cavagna A 2009 *Phys. Rep.* **476** 51
[2] Jung Y, Garrahan J P and Chandler D 2005 *J. Chem. Phys.* **123** 084509
[3] Goldstein M 2006 *J. Phys. Chem.* B **110** 9772
[4] Sastry S, Debenedetti P G and Stillinger F H 1998 *Nature* **393** 554
[5] Middleton T F and Wales D J 2003 *J. Chem. Phys.* **118** 4583
[6] Doliwa B and Heuer A 2003 *Phys. Rev.* E **67** 031506
[7] Fulcher G S 1925 *J. Am. Ceram. Soc.* **8** 339
[8] Vogel H 1921 *Z. Phys.* **22** 645
[9] Tammann G and Hesse W 1926 *Z. Anorg. Allg. Chem.* **156** 245
[10] de Souza V K and Wales D J 2006 *Phys. Rev.* B **74** 134202
[11] Mauro J C, Yue Y, Ellison A J, Gupta P K and Allan D C 2009 *Proc. Natl Acad. Sci. USA* **106** 19780
[12] Angell A 1998 *Nature* **393** 521
[13] Ito K, Moynihan C T and Angell C A 1999 *Nature* **398** 492
[14] Angell C A 1991 *J. Non-Cryst. Solids* **131–133** 13
[15] Greer A L, Kelton K F and Sastry S 2014 *Fragility of Glass-Forming Liquids* vol 13 (New Dehli: Hindustan Book Agency)
[16] Niblett S P, de Souza V K, Stevenson J D and Wales D J 2016 *J. Chem. Phys.* **145** 024505
[17] Niblett S P, Biedermann M, Wales D J and de Souza V K 2017 *J. Chem. Phys.* **147** 152726
[18] Banerjee A, Nandi M K and Bhattacharyya S M 2017 *J. Chem. Sci.* **129** 793
[19] Goldstein M 1969 *J. Chem. Phys.* **51** 3728
[20] Rabani E, Gezelter J D and Berne B J 1999 *Phys. Rev. Lett.* **82** 3649
[21] Heuer A, Doliwa B and Saksaengwijit A 2005 *Phys. Rev.* E **72** 021503
[22] de Souza V K and Wales D J 2008 *J. Chem. Phys.* **129** 164507
[23] Götze W 1999 *J. Phys.: Condens. Matter* **11** A1
[24] Hansen J-P and McDonald I R 1990 *Theory of Simple Liquids* (Amsterdam: Elsevier)
[25] Weeks J D, Chandler D and Andersen H C 1971 *J. Chem. Phys.* **54** 5237
[26] Berthier L and Tarjus G 2009 *Phys. Rev. Lett.* **103** 170601
[27] Pedersen U R, Schrøder T B and Dyre J C 2010 *Phys. Rev. Lett.* **105** 157801
[28] Banerjee A, Sengupta S, Sastry S and Bhattacharyya S M 2014 *Phys. Rev. Lett.* **113** 225701
[29] Berthier L and Tarjus G 2010 *Phys. Rev.* E **82** 031502
[30] Berthier L and Tarjus G 2011 *Eur. Phys. J.* E **34** 96
[31] Nandi M K, Banerjee A, Dasgupta C and Bhattacharyya S M 2017 *Phys. Rev. Lett.* **119** 265502
[32] Rosenfeld Y 2000 *Phys. Rev.* E **62** 7524
[33] Adam G and Gibbs J H 1965 *J. Chem. Phys.* **43** 139
[34] Banerjee A, Sevilla M, Rudzinski J F and Cortes-Huerto R 2021 arXiv:2107.04478
[35] Filion L, Ni R, Frenkel D and Dijkstra M 2011 *J. Chem. Phys.* **134** 134901
[36] Shendruk T N, Bertrand M, Harden J L, Slater G W and de Haan H W 2014 *J. Chem. Phys.* **141** 244910

[37] Kob W and Andersen H C 1995 *Phys. Rev.* E **51** 4626
[38] Scalliet C, Berthier L and Zamponi F 2019 *Nat. Commun.* **10** 5102
[39] Liu D C and Nocedal J 1989 *Math. Program.* **45** 503
[40] Trygubenko S A and Wales D J 2004 *J. Chem. Phys.* **120** 2082
[41] Sheppard D, Terrell R and Henkelman G 2008 *J. Chem. Phys.* **128** 134106
[42] Mills G, Jónsson H and Schenter G K 1995 *Surf. Sci.* **324** 305
[43] Jónsson H, Mills G and Jacobsen K W 1998 *Classical and Quantum Dynamics in Condensed Phase Simulations* ed ed B J Berne, G Ciccotti and D F Coker (Singapore: World Scientific) ch 16 pp 385–404
[44] Henkelman G, Uberuaga B P and Jónsson H 2000 *J. Chem. Phys.* **113** 9901
[45] Henkelman G and Jónsson H 2000 *J. Chem. Phys.* **113** 9978
[46] Munro L J and Wales D J 1999 *Phys. Rev.* B **59** 3969
[47] Kumeda Y, Wales D J and Munro L J 2001 *Chem. Phys. Lett.* **341** 185
[48] Carr J M, Trygubenko S A and Wales D J 2005 *J. Chem. Phys.* **122** 234903
[49] 2021 OPTIM: a program for geometry optimisation and pathway calculations (Cambridge UK: Wales group) http://wales.ch.cam.ac.uk/software.html

[50] Röder K and Wales D J 2020 *J. Chem. Phys.* **153** 034104
[51] Becker O M and Karplus M 1997 *J. Chem. Phys.* **106** 1495
[52] Wales D J, Miller M A and Walsh T R 1998 *Nature* **394** 758
[53] 2021 DisconnectionDPS: a program for creating disconnectivity graphs (Cambridge UK: Wales group) http://wales.ch.cam.ac.uk/software.html
[54] Keyes T 1997 *J. Phys. Chem.* A **101** 2921
[55] de Souza V K and Wales D J 2006 *Phys. Rev. Lett.* **96** 057802
[56] Banerjee A and Wales D J 2020 *J. Chem. Phys.* **153** 124501
[57] de Souza V K, Stevenson J D, Niblett S P, Farrell J D and Wales D J 2017 *J. Chem. Phys.* **146** 124103
[58] Berthier L and Tarjus G 2011 *J. Chem. Phys.* **134** 214503
[59] Sciortino F, Kob W and Tartaglia P 2000 *J. Phys.: Condens. Matter* **12** 6525
[60] Bogdan T V, Wales D J and Calvo F 2006 *J. Chem. Phys.* **124** 044102
[61] Wales D J 2013 *Chem. Phys. Lett.* **584** 1
[62] Banerjee A, Nandi M K, Sastry S and Bhattacharyya S M 2016 *J. Chem. Phys.* **145** 034502
[63] Athawale M V, Goel G, Ghosh T, Truskett T M and Garde S 2007 *Proc. Natl Acad. Sci. USA* **104** 733